Study on the Reduction Process of Iron Oxide Pellets in Isothermal Fixed Bed

Study on the Reduction Process of Iron Oxide Pellets in Isothermal Fixed Bed*

Jun-ichiro YAGI, Reijiro TAKAHASHI and Yasuo OMORI

The Research Institute of Mineral Dressing and Metallurgy

(Received July 7, 1971)

Synopsis

A mathematical model for the isothermal fixed bed and one of the numerical calculating method for this model are presented in this paper. The reaction rate accepted in this model is determined on the basis of the rate observed for single iron oxide pellet.

In order to clarify the availability of the mathematical model for analyzing the metallurgical reactors, change in the average fractional reduction over the whole bed with the progress of time was observed during the reduction of iron oxide pellets with CO and H_2 by the use of the experimental fixed bed. The observed data are in good agreement with the calculated curves except in the case where the pellets cracked badly during the reduction. It is, therefore, found that the distributions of process variables in isothermal fixed bed can be estimated with the considerable accuracy by the model mentioned above, and that the reaction rates of pellets with CO and H_2 used in this paper are expected to be available for the process analysis of metallurgical reactors.

I. Introduction

A number of kinetic studies on the metallurgical reactions such as indirect reduction of iron ores with CO, hydrogen reduction of iron ores, solution-loss reaction, and decomposition reaction of limestone were recently presented by various researchers.[(1)~(11)] The results on the rates of reactions mentioned above were applied to the process analysis of the moving bed, especially blast furance and

---

* The **197th** report of the Research Institute of Mineral Dressing and Metallurgy. Originally published in Japanese in Tetsu-to-Hagané, **57** (1971), 1453.

(1) Y. Hara, M. Tsuchiya and S. Kondo: Tetsu-to-Hagané, **55** (1969), 1297.
(2) T. Yagi and Y. Ono: Trans. Iron & Steel Inst. Japan, **8** (1968), 377.
(3) M. Taniguchi, T. Kubo and I. Muchi: Tetsu-to-Hagané, **56** (1970), 156.
(4) T. Yagi, Y. Ono and K. Kuwano: Tetsu-to-Hagané, **52** (1967), 1315.
(5) M.A. Osman, F.S. Manning and W.O. Philbrook: Am. Inst. Chem. Engrs. J., **12** (1966), 685.
(6) N. Miyasaka and S. Kondo: Tetsu-to-Hagané, **54** (1968), 1427.
(7) I. Muchi, J. Yagi, K. Tamura and A. Moriyama: J. Japan Inst. Metals, **30** (1966), 826.
(8) G. Heynert und J. Willems: Stahl und Eisen, **79** (1959), 1545.
(9) J. Yagi, K. Tamura and I. Muchi: J. Japan Inst. Metals, **31** (1967), 103.
(10) G. Narshimhan: Chem. Eng. Sci., **16** (1961), 7.
(11) T. Mamuro and T. Kitagawa: Preprint of 6th General Symposium, Soc. Chem. Engrs., Japan (1967), 120, Nagoya.

some useful informations concerning the operating characteristics of the process were obtained.

However, the process analysis of the fixed bed in which noncatalytic reactions are carried out is generally more difficult than that of moving bed. Few attempts, therefore, made to analyze the noncatalytic reaction process in the fixed bed, hitherto. On the other hand, the behavior of the fixed bed in which catalytic reactions are carried out were examined by various authors. This is understood by the following reasons. For catalytic reactions, steady-state is obtained in the isothermal fixed bed if solid catalysts do not change during the reaction. For noncatalytic reactions, however, steady-state can not be attained.

Accordingly, the one dimensional model for isothermal fixed bed in which catalytic reaction takes place is described mathematically by a set of ordinary differential equations. Whereas, one dimensional mathematical expression for isothermal fixed bed in which noncatalytic reaction proceeds is given by a set of partial differential equations. The analysis of the latter is, therefore, more difficult than that of the former.

Moriyama[12] solved analytically a set of partial differential equations which were derived for noncatalytic reaction by taking material balances of gas and solid particles in isothermal fixed bed and represented the solution for the longitudinal distribution of fractional reduction of solid particles.

Theoretical analysis on sintering process which was essentially considered as a fixed bed was made and numerical solutions for the distributions of process variables were given by Muchi and Higuchi[13], and Tsukamoto et al.[14]

As for the study on the reduction of iron oxides in the fixed bed with CO or H_2, the experimental result for the longitudinal distribution of the concentration of CO_2 was only reported by Privalov et al.[15]

In the present paper, one dimensional mathematical model for isothermal fixed bed is developed on the assumption that the reduction rate of single iron oxide pellet may be discribed by the unreacted core model. Applying the rate constant[16],[17] observed for single iron oxide pellet to this model, numerical solutions for the changes in fractional reduction of iron oxide pellet and concentration of CO at any level in the fixed bed with the progress of time are computed by the method of characteristic curves. The average reduction curves observed in the fixed beds having the various heights of bed are compared with those estimated by

(12) A. Moriyama: Chem. Eng., Japan, **34** (1970), 1308.
(13) I. Muchi and J. Higuchi: Tetsu-to-Hagané, **56** (1970), 371.
(14) T. Tsukamoto, S. Shimada, T. Tanaka and J. Higuchi: Tetsu-to-Hagané, **56** (1970), 661.
(15) S.I. Privalov, V.N. Timofeev and B.A. Bokovikov: Stal in English, (1960), 4.
(16) H. Shimamura, T. Terui, Y. Omori and K. Sanbongi: Tetsu-to-Hagané, **56** (1970), 1594.
(17) R. Takahashi, J. Yagi and Y. Omori: Tetsu-to-Hagané, **57** (1971), 1597: Sci. Rep. RITU, **A23** (1971), 9.

the theoretical calculations.

II. Mathematical model for isothermal fixed bed

In the process analysis of the reactors, it is, in general, necessary to consider both radial and longitudinal distributions of process variables such as temperatures of fluid and solid particles, concentration of fluid, fractional conversion of solid particles and voidage in the bed. Since great interest of the authors is focussed on the longitudinal distributions of the concentration of gas and fractional reduction of solid particles in the fixed bed, both temperature and voidage are assumed to be kept constant over the whole bed and the velocity profile is also assumed to be flat so that all radial gradients with respect to the process variables may be neglected. Under these circumstances, the reduction of iron oxide pellet with CO or H_2 given by Eqs. (1) and (2) in the fixed bed is analyzed.

$$(1/3)\,Fe_2O_3+CO=(2/3)\,Fe+CO_2 \tag{1}$$

$$(1/3)\,Fe_2O_3+H_2=(2/3)\,Fe+H_2O \tag{2}$$

The assumptions mentioned above may be justified by the facts that heat of reaction accompanied with each reaction given by Eqs. (1) and (2) is only a small quantity and that the diameter of reaction tube used in our experiment is not so large as described later.

On the basis of these assumptions, one dimensional fundamental equations (3) and (4) are derived by taking material balances for gas and solid particles around the differential height of bed, dz, at an arbitrary position from the bottom of the fixed bed as illustrated in Fig. 1.

$$u_0\,\partial c/\partial z+\varepsilon_b\,\partial c/\partial t=-R^* \tag{3}$$

$$\partial f/\partial t=R^*/(1-\varepsilon_b)\,\rho_s a \tag{4}$$

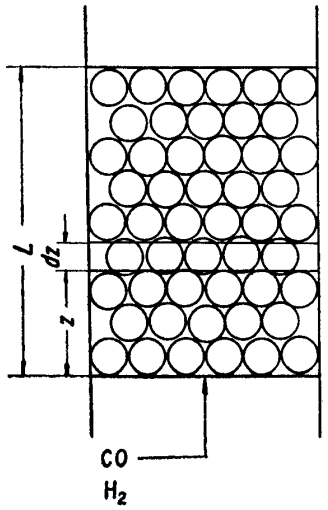

Fig. 1. Schematic profile of fixed bed for taking material balances.

Initial and boundary conditions for Eqs. (3) and (4) are given by Eq. (5).

$$\left.\begin{aligned} &f=0, \quad c=C^* && \text{at } t=0 \\ &c=c_0 && \text{at } z=0 \end{aligned}\right\} \tag{5}$$

Namely, one dimensional model for isothermal fixed bed in which noncatalytic reaction takes place is described by two simultaneous partial differential equations. These partial differential equations include the overall reduction rate of iron oxide pellets per unit volume of bed, R^*. According to the unreacted core model[17] which is often used to the expression of the reduction rate of iron oxide with gas, R^*, is given by Eq. (6).

$$R^* = \frac{3(1-\varepsilon_b)(c-C^*)/\phi r_0}{1/k_f + r_0(r_0-r_i)/r_i D_s + r_0^2/r_i^2 k(1+1/K)} \tag{6}$$

Now, the following dimensionless variables are introduced and then Eqs. (7) and (8) are obtained as dimensionless expression for Eqs. (3) and (4).

$$z/L=\eta, \quad ut/L=\theta, \quad (c-C^*)/(c_0-C^*)=\chi$$

$$3(1-\varepsilon_b)Lk_f/\phi r_0 u_0=\alpha, \quad 3(1-\varepsilon_b)LD_s/\phi r_0^2 u_0=\beta$$

$$3(1-\varepsilon_b)Lk(1+1/K)/\phi r_0 u_0=\delta, \quad \phi\varepsilon_b(c_0-C^*)/(1-\varepsilon_b)\rho_s a=\varphi$$

$$\partial\chi/\partial\theta+\partial\chi/\partial\eta=-R(f)\chi \tag{7}$$

$$\partial f/\partial\theta=\varphi R(f)\chi \tag{8}$$

$$R(f)=1/[1/\alpha+(1/\beta)\{(1-f)^{-1/3}-1\}+(1/\delta)(1-f)^{-2/3}] \tag{9}$$

Eq. (10) is derived as the dimensionless expressions of initial and boundary conditions from Eq. (5).

$$\left.\begin{aligned} &f=0, \quad \chi=0 && \text{at } \theta=0 \\ &\chi=1 && \text{at } \eta=0 \end{aligned}\right\} \tag{10}$$

Longitudinal distributions of χ and f can be calculated at an arbitrary time, θ, by solving Eqs. (7) to (9) under the initial and boundary conditions given by Eq. (10).

III. Numerical analysis

Approximate analytical solution for the fundamental equations given by Eqs. (7) to (9) has been presented by Moriyama.[12] In this paper, numerical solutions for the fundamental equations are obtained by the method of characteristics. Some attention should be paid to the fact that this numerical method can also be applied to solving the fundamental equations mentioned above in the case where any expression for reaction rate, R^*, is introduced instead of Eq. (6) and to the analysis of the nonisothermal process.

According to this method, the partial differential equations given by Eqs.

(7) and (8) are changed into the ordinary differential equations given by Eqs. (13) and (14), since Eqs. (7) and (8) are integrated along the characteristic curves expressed by Eqs. (11) and (12), respectively.

$$d\theta/d\eta = 1 \tag{11}$$

$$d\eta/d\theta = 0 \tag{12}$$

$$d\chi/d\eta = -R(f)\chi \tag{13}$$

$$df/d\theta = \varphi R(f)\chi \tag{14}$$

Eqs. (11′) and (12′) are obtained by integrating Eqs. (11) and (12), respectively.

$$\theta = \eta + \text{const} \tag{11'}$$

$$\eta = \text{const} \tag{12'}$$

It is, therefore, found from Eqs. (11′) and (12′) that Eq. (13) must be integrated to the direction of gas flow and that Eq. (14) must be integrated to the direction of time at any position in the bed. The integral paths for Eqs. (13) and (14) are illustrated in Fig. 2.

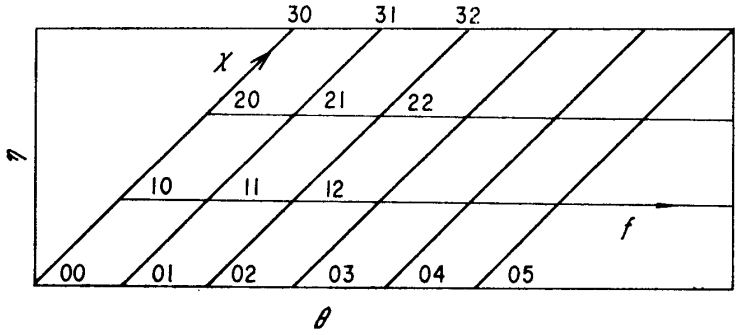

Fig. 2. Network of two characteristic curves given by Eqs. (11) and (12)

On the basis of Eq. (10), initial and boundary conditions for Eqs. (13) and (14) are derived as follows (referring to appendix):

Initial conditions at $\eta=\theta$:

$$f = 0$$

$$\chi = \exp\{-\delta\alpha/(\alpha+\delta)\}$$

Boundary conditions at $\eta=0$:

$$\left.\begin{array}{ll} \chi = 1 & \text{for all } \theta \\ \varphi\theta = f(1/\alpha - 1/\beta) + 3\{1-(1-f)^{2/3}\}/2\beta + 3\{1-(1-f)^{1/3}\}/\delta & \text{for } \theta < \theta_c \\ f = 1 & \text{for } \theta \geq \theta_c \end{array}\right\} \tag{16}$$

where,

$$\theta_c = (1/\alpha + 1/2\beta + 3/\delta)/\varphi \tag{17}$$

By using these initial and boundary conditions, Eqs. (13) and (14) can be solved numerically. In the numerical calculations, it would be desirable not only to obtain stable solutions with the allowable errors but also to shorten the computing time.

In this paper, when the differentials in Eqs. (13) and (14) were replaced by small finite increments, about one diameter of the particle was chosen as the finite increment for longitudinal distance ($\Delta\eta$), whereas, the finite increment for time ($\Delta\theta$) was determined to be 20 times as long as the time ($\Delta\tau$) required for gas to flow through an finite increment for longitudinal distance ($\Delta\eta$) in earlier stage of the reduction process and at $100\Delta\theta$ and $1000\Delta\theta$ in reduction times, it was increased to $40\Delta\tau$ and $100\Delta\tau$ respectively. This treatment was due to the following reasons: As the derivatives of χ and f with respect to θ fell gradually at any level in the bed in the latter stage of the reduction process, the increase in $\Delta\theta$ did not lead to the growth of the error. Therefore, it was increased for shortening the computing time. Runge-Kutta-Gill method was employed to the numerical integration.

In addition, for the purpose of investigating both truncation and round off errors in numerical computation, numerical solutions were obtained under the same operating conditions in the cases where $\Delta\eta$ was decreased to $d_p/2$ and where $\Delta\theta$ was increased to $50\Delta\tau$ in the initial stage of the reduction process and at $100\Delta\tau$ and $1000\Delta\theta$ in reduction times, it was also increased to $100\Delta\theta$ and $250\Delta\tau$. The numerical solutions computed under these finite increments were essentially identical with that computed under the finite increments for time and distance mentioned earlier. Both truncation and round off errors may be neglected under these finite increments.

Numerical computation was conducted by use of the digital computer NEAC model 500 in 2200 series in Tohoku University and only 3 minutes were required for obtaining the numerical solution in the case where the number of distance increments was equal to 5 and reducing time was about 60 minutes.

IV. Experiments.

The experimental apparatus used in this paper was the same as used by Shimamura et al.[16] to examine the reduction test method for various iron oxides. This apparatus was made on the basis of the reduction test method recommended by JIS (Japan Industrial Standard). The inner diameter of 8.3 cm is, however, slightly larger than that of JIS (7.5 cm), another difference is the adoption of a spiral tube for preheating the inlet gas in order to keep the isothermal condition.

Both CO and H_2 was used as reducing gas and in each case, N_2 was introduced to dilute the molar fraction of reducing gas to 0.4.

The pellets subjected to the experiment had apparent density of 4.12 g/cm^3 and porosity of 0.16, and chemical composition of the pellets is indicated in Table 1. Various amounts of the pellets which had the uniform diameter within the error limit of ± 1 mm were packed in the reaction tube and after measuring

Table 1. Chemical composition of the pellet (wt%)

T·Fe	FeO	SiO_2	CaO	Al_2O_3	MgO	S
65.07	1.37	4.04	0.62	1.23	0.58	0.004

the height of bed, reduction curves were observed by weight loss.

In the case of the reduction with CO, changes in the average fractional reduction over the whole bed with the progress of time had been observed by Shimamura et al.[16] for two kinds of fixed bed containing the pellets of 300 and 1050 g. Thus, same observation was conducted with the fixed bed containing the pellets of 500 g by the authors. On the other hand, in the case of the reduction with H_2, changes in the average fractional reduction with the progress of time were observed for two kinds of fixed bed containing the pellets of 642 and 1005 g.

V. Reduction of single iron oxide pellet

1. Reduction rate of single iron oxide pellet with CO

As for the reduction with CO described by Eq. (1), Shimamura et al.[16] observed the reduction rate of the single pellet which had the same chemical composition as that used by the authors for analyzing the reduction process in the fixed bed in this paper. According to the unreacted core model considering three processes of diffusion through gaseous film, intraparticle diffusion and chemical reaction, the experimental data reported by Shimamura et al.[16] were analyzed and the values of the rate constant, k, obtained under various conditions are plotted against reciprocal temperature as shown in Fig. 3. From Fig. 3, the observed values seem to be expressed by a linear function of reciprocal temperature.

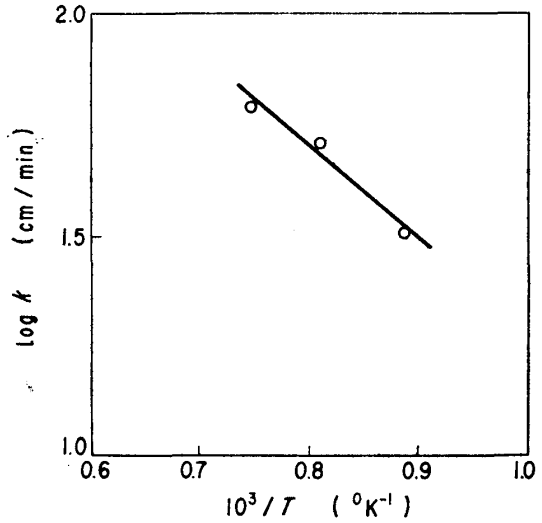

Fig. 3. Temperature dependency of the reaction rate constants of the pellets with CO observed by Shimamura et al.[16]

Thus, following expression for temperature dependence of the reaction rate constant is obtained by the method of least squares.

$$k = \exp(7.60 - 9100/RT) \qquad \text{(cm/min)} \tag{18}$$

The activation energy for k is about 9.1 kcal/mol and this value is in the same magnitude of those reported by other investigators.

Equilibrium constant, K, mass transfer coefficient through gaseous film, k_f, and intraparticle diffusivity, D_s, are required in calculating the reaction rate constant. For evaluating the value of K for the reduction of iron oxide, Eq. (19) which gives the equilibrium constant for the system of $FeO/Fe/H_2$-H_2O is introduced.

$$K = \exp(-2.642 + 2.164/T) \qquad T > 848°K \tag{19}$$

The expression for mass transfer coefficient through gaseous film, k_f, is given as Eq. (20) which was proposed by Ranz and Marshall.[18]

$$Sh = 2.0 + 0.6\,(Re_p)^{1/2}\,(Sc)^{1/3} \tag{20}$$

Density of gas mixture contained in Eq. (20) is calculated from that of each component on assumption of additivity. Viscosity of gas mixture is obtained from Licht-Stecherts equation[19] based on the principle of corresponding state. Regarding the diffusivity of CO, the diffusivity of CO in binary gas system of CO and N_2 is estimated from Andrussow's equation[20] and the value is used in place of the value for diffusivity of CO in ternary gas system of CO, CO_2 and N_2, because concentration dependence for diffusivity may be neglected. The equations used for estimations of viscosity and diffusivity are known to agree well with respective experimental data.

Intraparticle diffusitivty, D_s, is evaluated from Eq. (21) expressed by using porosity and labyrinth factor of reduced iron layer.

$$D_s = D\,\xi\,\varepsilon_v \tag{21}$$

On the assumption of the unchanging size of the pellet during the reduction, porosity of reduced iron layer is obtained from Eq. (22)

$$\varepsilon_v = 0.53 + 0.47\,\varepsilon_p \tag{22}$$

Labyrinth factor is calculated from Eq. (23) indicated as a linear function of temperature in the previous paper.[18]

$$\xi = 4.4 \times 10^{-4}(T - 773) + 0.18 \qquad (T > 773) \tag{23}$$

In order to examine whether the evaluated values for k_f, D_s, k and K are appropriate to the experimental results or not, Eq. (6) was integrated under constant $(c\text{-}C^*)$ and the relationship between f and t obtained by theoretical

(18) W.E. Ranz and W.R. Marshall: Chem. Eng. Progr., **48** (1952), 141.
(19) W. Licht and D.G. Stechert Jr.: J. Phys. Chem., **48** (1944), 23.
(20) K. Sato: Chem. Eng., Japan, **28** (1964), 490.

treatment is compared with observed data as shown in Fig. 4. In Fig. 4, slightly different trend is found between theoretical and observed reduction curves. Namely, in the initial stage of the reduction process, calculated reduction curves shows more rapid rate than observed one, and in latter stage, however, observed fractional reduction is slightly higher than calculated one. This trend is explained qualitatively as follows: Observed reudction curve is similar to the sigmoidal fashion due to the reasons that the reduction of the single pellet with CO have induction period in the initial stage and have the trend of rapid progress in reduction in the middle stage, but theoretical reduction curves gives the smooth one since the induction period and the rapid progress of reduction occurred in middle stage are out of account in the unreacted core model defined by Eq. (6). However, Fig. 4 shows the satisfactory accordance between observed and calculated reduction curves. Consequently, from the viewpoint of the reproduction of the reduction curve, the reasonable values for rate parameters of k_f, D_s and k, and for equilibrium constant K, may be estimated from Eqs. (8) to (23).

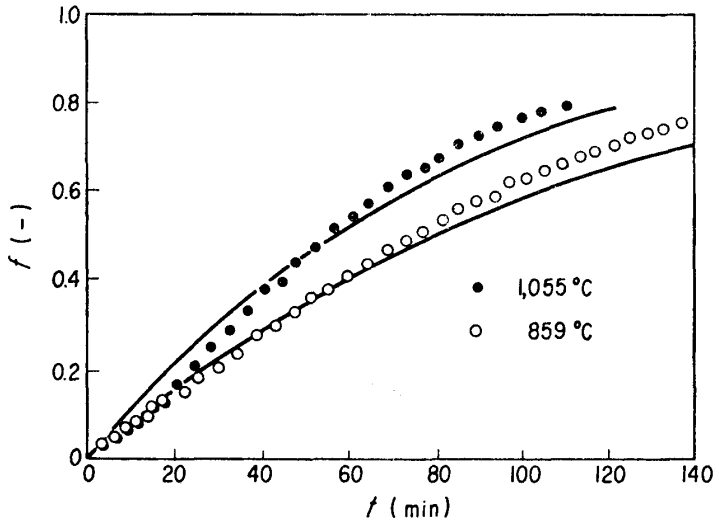

Fig. 4. Comparison of calculated curves with experimental data observed by Shimamura et al.[16] in the reduction of single pellet with CO.

2. Reduction rate of single iron oxide pellet with H_2

The reduction test of single iron oxide pellet with gas mixture of H_2 and N_2 was conducted and the observed data were analyzed by the authors[17] for evaluating the rate parameters k_f, D_s and k, and equilibrium constant, K, in a manner similar to the method mentioned in the previous paragraph. According to the report, following expressions were obtained for reaction rate and equilibrium constants in regard to the hydrogen-reduction given by Eq. (2).

$$k = \exp(16.2-25.7\times 10^3/RT) \qquad \text{(cm/min)} \qquad (24)$$

$$K = \exp(1.0837-1737.2/T) \qquad (25)$$

The activation energy for k is about 26 kcal/mole and this value is slightly higher than previously reported values which were obtained by other researchers in assuming the chemical reaction control. The other rate parameters, k_f and D_s, can be determined by using the equations described in this paper.

VI. Reduction of iron oxide pellets in the fixed bed

1. Reduction of pellets with CO in the fixed bed

The average fractional reduction over the whole bed observed by the use of the fixed bed including the various amounts of pellets and the theortical curves obtained by numerical analysis mentioned in the previous paragraph are shown in Figs. 5 to 7. The observed data with the fixed bed containing the pellets of 300 and 1050 g illustrated in Figs. 5 and 7 were reported by Shimamura et al.[16] and the data for the pellets of 500 g shown in Fig. 6 were observed by the authors.

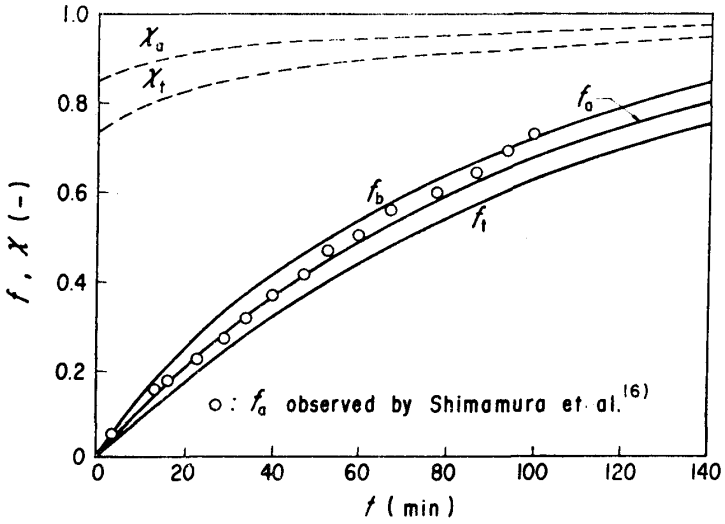

Fig. 5. Comparisons of calculated curves of f with experimental data in the reduction of the pellets with CO in the fixed bed under the condition of $L=2.52$(cm), $W_p=300$ (g), $T=1055$ (°C), $d_p=1.2$ (cm), $F=59$ (Nl/min), $\varepsilon_b=0.466$.

In Figs. 5 to 7, the increase in amount of pellets packed in the fixed bed leads to the increase in height of bed and it is 2.5 cm for Fig. 5, 4.2 cm for Fig. 6, and 8.0 cm for Fig. 7. For all cases, the flow rate of gas is 59 Nl/min and inlet gas has the composition of CO (40%) and N_2 (60%). The reduction temperature is 1055° C for Fig. 5 and is 957°C for Figs. 6 and 7. Void fraction in the fixed bed was calculated by use of the bed volume and the volume occupied by the pellets which was obtained from the total weight and apparent density of packed pellets.

In Fig. 5, the height of bed is low so that no significant difference in the fractional reductions between top and bottom levels in the fixed bed may be found. However, observed data almost coincide with the theoretical curves. Changes in the concentrations of CO averaged over the whole bed and at the top level of the

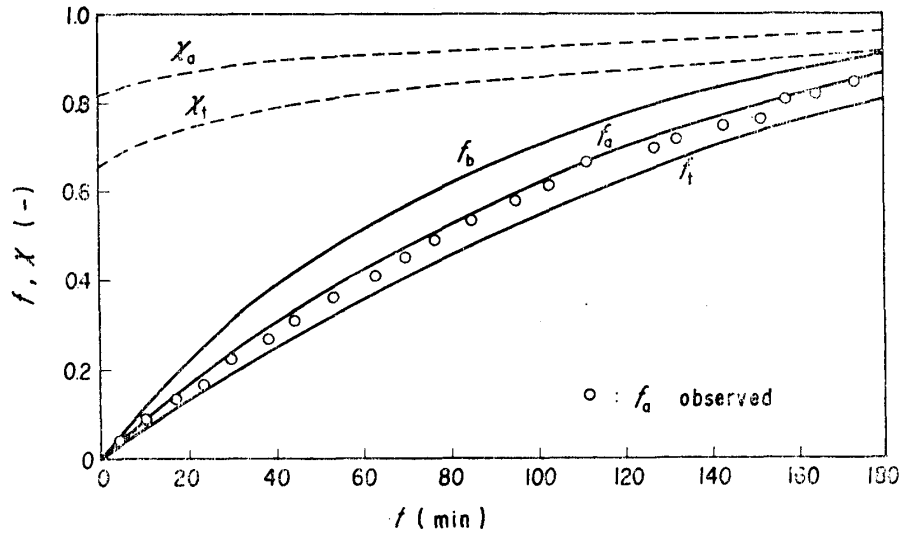

Fig. 6. Comparisons of calculated curves of f with experimental data in the reduction of the pellets with CO in the fixed bed under the condition of $L=4.2$ (cm), $W_p=500$ (g), $T=957$ (°C), $d_p=1.2$ (cm), $F=59$ (Nl/min), $\varepsilon_b=0.466$.

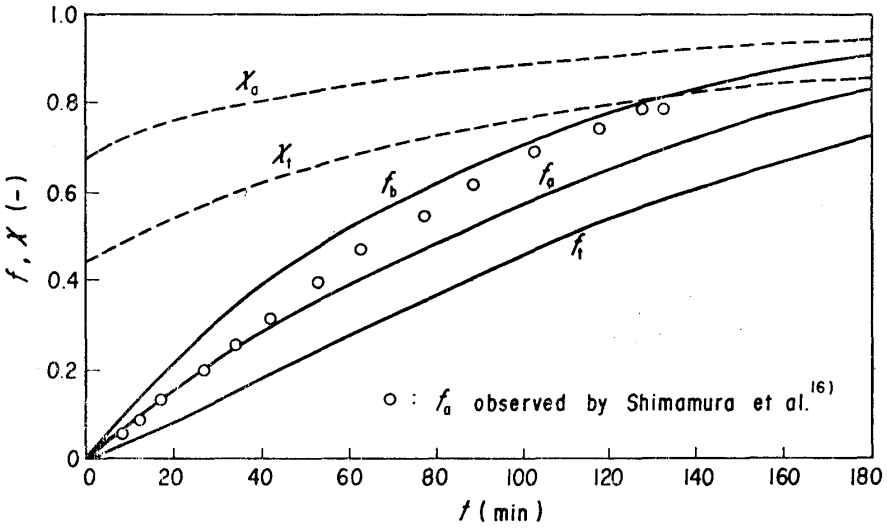

Fig. 7. Comparisons of calculated curves of f with experimental data in the reduction of the pellets with CO in the fixed bed under the condition of $L=8$ (cm), $W_p=1050$ (g), $T=957$ (°C), $d_p=1.2$ (cm), $F=59$ (Nl/min), $\varepsilon_b=0.410$.

bed are shown by dotted lines and the substantial difference between concentrations of CO at top and bottom levels did not also appear.

Fig. 6 gives the comparison of the observed data with calculated curves for fractional reduction averaged over the whole bed in the case where the weight of pellet amounts to 500 g and the height of bed is equal to 4.2 cm. Slight increase in the height of bed compared with Fig. 5 may cause the slight growth of the difference between the fractional reductions at top and bottom levels.

Corresponding to this phenomenon, the difference between the concentrations

of CO, χ, at top and bottom levels is also slightly increased. The observed values for f_a are in good agreement with the calculated curves.

Fig. 7 shows both observed and calculated results in the case where 1050 g of the pellets are packed in the bed and its altitude is equal to 8 cm. In this case, the experimental data indicate the considerably higher values than the calculated curves except in the early reduction stage. According to the observation of the pellets in the reaction tube after the experimental run, both cracking and degradation of pellets were scarcely found in the cases of the sample weight of 300 and 500 g, although swelling and sintering of pellets were somewhat occurred, but in the case of Fig. 7 substantial degradation of pellets was found in the upper part of the bed. Therefore, cracking and degradation of the pellets may lead to the poor agreement between experimental and theoretical values of f_a. The degradation of the pellets in the case of Fig. 7 may be caused by the following reasons. The gas in the upper part of the bed contains considerable amount of CO_2 in the early reduction stage, consequently, Fe_2O_3 may be easily reduced to FeO, however, not easily to iron. This phenomenon may cause the swelling and decrease in mechanical strength of pellets. It seems, therefore, that stress between particles or between wall and particle caused by swelling leads to cracking and degradation of pellets.

In addition, calculated curves of fractional reduction at the top and the bottom levels illustrated in Fig. 7 were obtained without consideration of cracking and degradation.

Fig. 8 gives the longitudinal distributions of fractional reduction and concentration of CO with time as a parameter under the same experimental conditions as Fig. 6. It is found from the distribution of fractional reduction that in the early reduction stage, the reduction proceeds rapidly in the lower part of

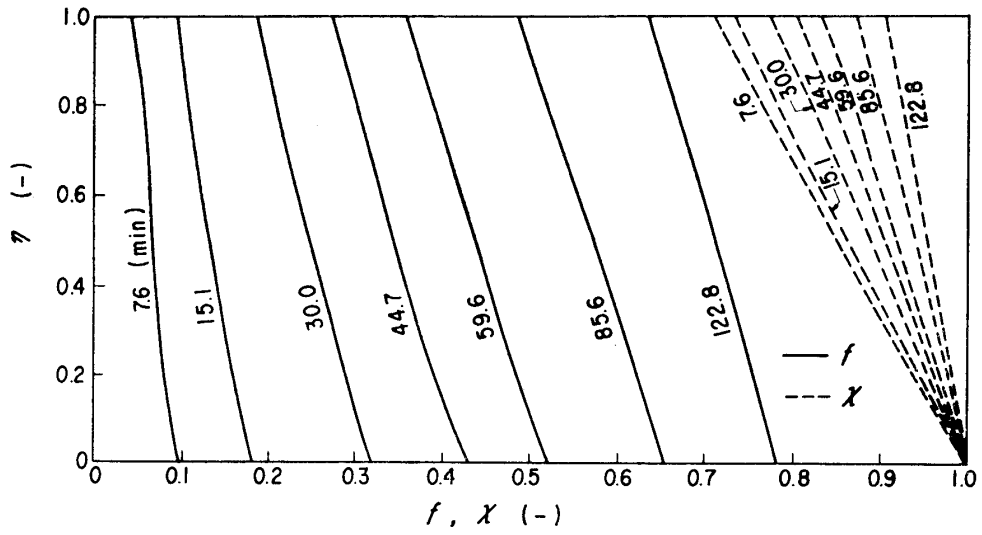

Fig. 8. Longitudinal distributions of f and χ with time as a parameter under the same calculating condition as Fig. 6.

the bed while proceeds slowly in the upper part of the bed, and in the middle reduction stage, the reduction rate is almost equal all over the bed. However, both the distributions of f and χ can be almost expressed by straight lines. This is understood qualitatively by the reasons that concentration of CO did not come close to the thermodynamic equilibrium and scarcely affect the reaction process because of the lower height of bed (4.2 cm) and the comparatively slow rate of the reduction of iron oxide pellet used.

2. Reduction of pellets with H_2 in the fixed bed

Packing the pellets of 642 and 1005 g in the reaction tube, changes in the fractional reduction of iron oxide pellets were observed with the progress of time, and both observed and calculated results are illustrated in Figs. 9. and 10. In Figs. 9 and 10, observed data for f_a almost coincide with the calculated curves, although the calculated curves are slightly heigher than observed data in both cases. Consequently, the theory mentioned in this paper can be applied to this system.

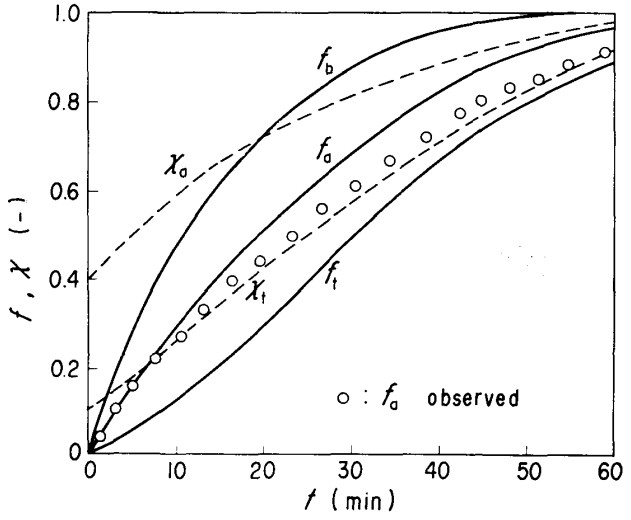

Fig. 9. Comparisons of calculated curves of f with experimental data in the reduction of the pellets with H_2 in the fixed bed under the condition of $L=5.1$ (cm), $W_p=642$ (g), $T=960$ (°C), $d_p=1.12$ (cm), $F=50$ (Nl/min), $\varepsilon_b=0.429$.

It may be explained by the following reasons that the calculated values of f_a are slightly higher than the observed data: The reaction given by Eq. (2) is endothermic even though heat of reaction accompanied with this reaction is small amount, and the reduction of the pellets with H_2 proceeds more rapid than with CO, therefore, the temperature in the fixed bed may be slightly decreased. As the result, the longitudinal distribution of fractional reduction is considered to depend strongly upon that of temperature, especially in the larger fixed bed. In comparisons of Figs. 9 and 10 with Figs. 5 to 7, the difference between f_b and f_t is larger in the reduction with H_2 than with CO. This phenomenon is explained

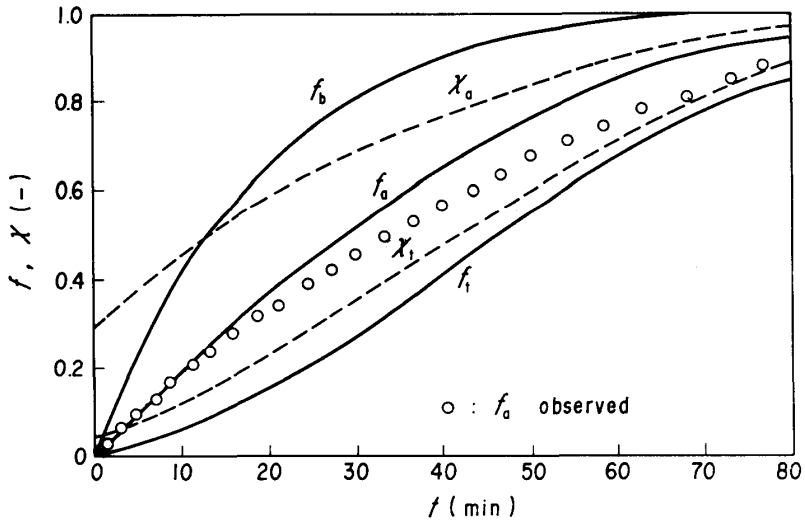

Fig. 10. Comparisons of calculated curves of f with experimental data in the reduction of the pellets with H_2 in the fixed bed under the condition of $L=7.6$ (cm), $W_p=1{,}005$ (g), $T=960$ (°C), $d_p=1.28$ (cm), $F=50$ (Nl/min), $\varepsilon_b=0.405$.

by the fact that the reduction of the pellet with H_2 proceeds more rapid than with CO.

In order to observe the reducing situation of the pellets in the fixed bed, at the reducing time of 78 minutes, N_2 was introduced into the fixed bed in which iron oxide pellets had been reduced with H_2 and after cooling the bed, samples of the pellets were taken at various levels in the bed. On the sampling of the pellets, the pellets could be pick up one by one because sintering of the pellets did not occur at all. The transverse sections of the pellets were taken a picture and shown in

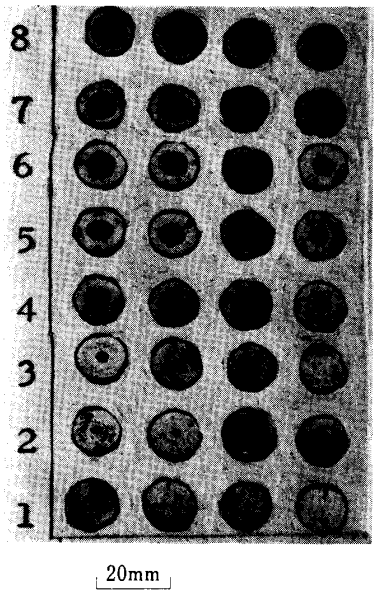

Photo. 1. Typical pattern for the reduction feature of pellets in the fixed bed.
1: at the bottom of the bed. 8: at the top of the bed.

Photo. 1. The reduction curve observed in this case is shown in Fig. 10. In Photo. 1, the pellets at first and second levels from the bottom of the bed is almost completely reduced and with the approach to the top level of the bed, the amount of unreacted core in the pellets is increased, and thus at the top level of the bed, the pellets are reduced about 80 percent only. These results obtained by the observation of the pellets in the fixed bed agree well with the calculated values of f_b and f_t at the reduction time of 78 minutes illustrated in Fig. 10.

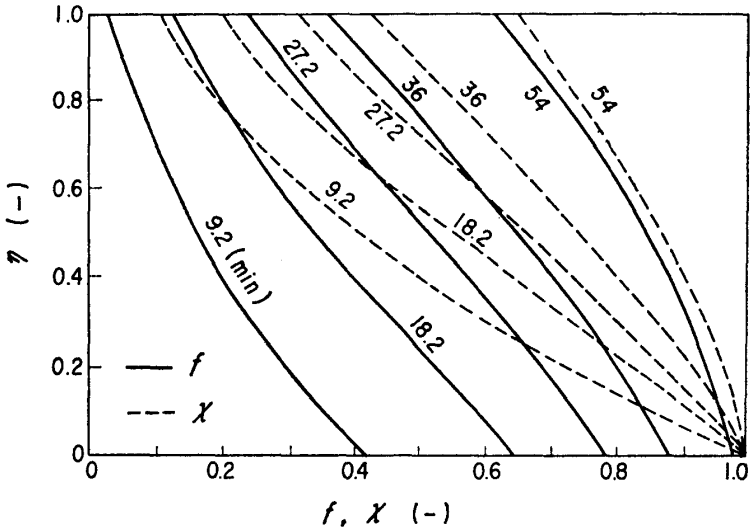

Fig. 11. Longitudinal distributions of f and χ with time as a parameter under the same calculating condition as Fig. 9.

Fig. 11 gives the longitudinal distributions of f and χ obtained by the mathematical model under the same operating condition as Fig. 9. In Fig. 11, both f and χ show considerable changes in the bed. In the early stage of the reduction, both f and χ show abrupt changes near the bottom of the bed because of the rapid progress of the reduction, however, along with the approach to the top of the bed, changes in f and χ decrease since concentration of H_2 comes close to the thermodynamic equilibrium. With the progress of time, the pellets existing near the bottom of the bed are reduced rapidly to higher fractional reduction so that the reduction rate becomes gradually slow. Therefore, the part of the steepest slope in the curve for f moves gradually upwards. At the same time, the slope of χ decreases near the bottom of the bed, conversely, increases near the top of the bed.

VII. Conclusion

A mathematical model for the isothermal fixed bed and one of the calculating method are presented in this paper. The reaction rate accepted in this model is determined on the basis of the rate observed for single iron oxide pellet.

Changes in the average fractional reductions over the whole bed were observed with the progress of time during the reduction of iron oxide pellets with CO and H_2 by the use of the experimental fixed bed and the observed data are in good agreement with the calculated curves except in the case where the pellets crack badly during the reduction. It is, therefore, found that the distributions of process variables in isothermal fixed bed can be estimated with the considerable accuracy by this model and that the reaction rates of the pellets with CO and H_2 used in this paper are expected to be available for the process analysis of metallurgical reactors. In addition, the numerical analysis of the fundamental equations presented in this paper can be applied to the analysis of nonisothermal process.

Besides, in the reduction of iron oxide pellets, longitudinal distributions of fractional reduction and of concentration of reducing gas exist even in the fixed bed of the low altitude and exert considerable influence on the reduction process. Therefore, it may be better that reduction rate of the iron oxide pellet is observed with single particle.

Nomenclature

a	stoichiometric constant
C^*	equilibrium concentration of reducing gas, (moles/cm^3)
c, c_0	concentration of reducing gas at any level in the bed and at the bottom of the bed, (moles/cm^3)
D_s	intraparticle diffusivity, (cm^2/min)
d_p	diameter of the pellet, (cm)
F	flow rate of gas, (Nl/min)
f, f_b, f_t	fractional reduction of the pellet at any level in the bed, at the bottom of the bed and at the top of the bed respectively
f_a	average fractional reduction of the pellets over the whole bed
K	equilibrium constant
k	reaction rate constant, (cm/min)
k_f	mass transfer coefficient through gaseous film, (cm/min)
L	height of bed, (cm)
R	gas constant, (cal/mol·°K)
R^*	reaction rate per unit volume of the bed, (moles/cm^3 (bed)·min)
r_i	interfacial radius in the pellet, (cm)
r_0	radius of the pellet, (cm)
T	temperature, (°K)
t	time, (min)
u_0	superficial velocity of gas, (cm/min)
W_p	weight of particles packed in the reaction tube, (g)
z	longitudinal distance from the bottom of the bed, (cm)

$\alpha, \beta, \delta, \varphi$	dimensionless variables
ε_b	void fraction of the fixed bed
$\varepsilon_v, \varepsilon_p$	porosity of reduced iron layer and of unreacted particle respectively
η	dimensionless distance
θ	dimensionless time
ρ_s	apparent density of the pellet, (g/cm^3 (solid))
χ, χ_t	dimensionless concentration of reducing gas at any level in the bed and at the top level of the bed respectively
χ_a	average dimensionless concentration of reducing gas over the whole bed

Appendix

Mathematical derivation of both initial and boundary conditions for the fundamental equations (13) and (14) is presented below.

As for the initial condition for χ, Eq. (i) is obtained by substituting $f=0$ at $\eta=\theta$ in Eq. (13).

$$d\chi/d\eta = -R(0)\chi \tag{i}$$

Following expression for χ can be derived by integrating Eq. (i) by use of Eq. (9).

$$\chi = \exp\{-\alpha\delta/(\alpha+\delta)\} \tag{ii}$$

As for the boundary condition for f, substitution of $\chi=1$ at $\eta=0$ in Eq. (14) gives Eq. (iii).

$$df/d\theta = \varphi R(f) \tag{iii}$$

In the case where the operating time is shorter than the time for complete reduction of the pellet at the bottom of the bed (θ_c), integration of Eq. (iii) by use of Eq. (9) gives Eq. (iv) which represents the relationship between θ and f.

$$\varphi\theta = f(1/\alpha - 1/\beta) + 3\{1-(1-f)^{2/3}\}/2\beta + 3\{1-(1-f)^{1/3}\}/\delta \tag{iv}$$

In the case where the operating time exceeds θ_c, value of f is equal to 1 at $\eta=0$.

In addition, the expression for θ_c is given by Eq. (v) which is obtained by putting $f=1$ in Eq. (iv).

$$\theta_c = (1/\alpha + 1/2\beta + 3/\delta)/\varphi \tag{v}$$